Journal of Materials Chemistry

Dynamic Article Links

Cite this: J. Mater. Chem., 2011, 21, 17345

www.rsc.org/materials

PAPER

Novel bis-C_{60} derivative compared to other fullerene bis-adducts in high efficiency polymer photovoltaic cells†

Eszter Voroshazi,*[ab] Karolien Vasseur,[ac] Tom Aernouts,[a] Paul Heremans,[ab] Andreas Baumann,[d] Carsten Deibel,[d] Xiang Xue,[e] Angela J. Herring,[e] Andreas J. Athans,[e] Tom A. Lada,[e] Henning Richter[e] and Barry P. Rand[a]

Received 24th May 2011, Accepted 9th August 2011
DOI: 10.1039/c1jm12307f

We report the application of novel mono- and bis-o-quino-dimethane C_{60} (oQDMC$_{60}$) adducts in bulk heterojunction photovoltaic devices. When blended with poly(3-hexylthiophene), the fullerene adducts presented here have an enhanced open-circuit voltage of 640 mV and 820 mV, while preserving high short-circuit current and fill factor, resulting in efficiencies of 4.1% and 5.2%, respectively. Detailed assessment of material properties relevant to photovoltaic devices such as energy levels, charge carrier mobility, absorption and solubility further complements the evaluation. Increased fullerene solubility hindering phase segregation in blends with bis-oQDMC$_{60}$ has been circumvented by an in-depth morphology optimization assisted by absorption spectroscopy, X-ray reflectivity and atomic force microscopy. This optimized preparation could also serve as a guide for implementation of similar fullerene derivatives. Furthermore, we compare bis-oQDMC$_{60}$ to previously reported fullerene bis-adducts to provide insight into this emerging class of materials.

1. Introduction

The efficiency of organic photovoltaic devices has swiftly risen in the last years to values of over 8% for single-junction polymer: fullerene bulk heterojunction cells.[1,2] Important advances in the understanding of structure-property relationships of donor-type conjugated polymers as well as the identification of promising polymer types have largely driven this progress.[3] Despite considerable effort in acceptor-type polymer and small molecule synthesis, fullerene derivatives remain the most efficient acceptor materials in these blends.[4] This unmatched performance of C_{60} derivatives stems from the combination of their desirable frontier orbital energetics, enabling efficient charge transfer, combined with their high electron mobility owing to their ability to self-organize into percolating pathways for charge collection. However, the commonly used phenyl-C_{61}-butyric acid methyl ester (PCBM) acceptor presents several limitations, namely reduced absorption in the visible region and a deep lowest unoccupied molecular orbital (LUMO) compared to polymers such as poly(3-hexylthiophene) (P3HT). To enable enhanced efficiencies, optimization of the offset between the LUMO of the donor and acceptor should balance more efficient charge transfer with reduced open-circuit voltage (V_{OC}). The former process requires the acceptor's LUMO to have a sufficient offset compared to the donor's LUMO to ensure an exothermic electron transfer.[5] On the other hand, the maximum V_{OC} in bulk heterojunctions is determined by the difference of the donor's highest occupied molecular orbital (HOMO) and the fullerene's LUMO, provided the electrical contacts are ohmic.[6] An optimum LUMO offset emerges as result of these considerations. This quest to determine the optimal LUMO offset has mostly focused on the archetypal P3HT:PCBM material system, where an offset larger than 700 meV clearly limits the photovoltage.

Molecular design of sidechains attached to C_{60} proves to be a successful pathway to tune frontier energy levels, though modifications preserving good charge transport and morphology, as well as solubility, are challenging.[7,8] Compared to PCBM, the most promising molecules in combination with P3HT presented an increase of 70 mV,[9] 140 mV,[10] 230 mV[11] and 260 mV[12,13] in V_{OC}, with nearly no change to the other photovoltaic parameters after optimization, producing efficiencies of 4.5%, 5.8% and 5.6% (up to 6.5%[14]), respectively. The highest V_{OC} of 890 mV in P3HT:fullerene devices was reached with trimetallic nitride endohedral fullerenes, though a decrease in photocurrent inhibited an overall efficiency enhancement.[15,16] Currently, one of the most successful design routes to raise the

[a]*IMEC, Organic Photovoltaics, Kapeldreef 75, Leuven, Belgium*
[b]*Katholieke Universiteit Leuven, ESAT/MICAS, Arenberg Kasteelpark 10, Leuven, Belgium*
[c]*Katholieke Universiteit Leuven, MTM, Arenberg Kasteelpark 44, Leuven, Belgium*
[d]*Experimental Physics VI, Julius-Maximilians-University of Würzburg, Würzburg, Germany*
[e]*NanoC Inc., Southwest Park 33, Westwood, MA, USA*
† Electronic supplementary information (ESI) available. See DOI: 10.1039/c1jm12307f

fullerene's LUMO level is the multiple adduction of identical sidechains on the C_{60} cage.[10,14] However, these bulkier molecules both inhibit close packing with the polymer and introduce energetic disorder, as synthesis inherently yields a mixture of their numerous isomers.[17,18]

Here, we report the characterization and evaluation in photovoltaic cells of mono-o-quino-dimethane C_{60} (mono-oQDMC$_{60}$) and bis-o-quino-dimethane C_{60} (bis-oQDMC$_{60}$) yielding 4.1% and 5.2% efficient devices in blends with P3HT, respectively. These novel mono- and bis-adduct fullerenes have compact sidechains that raise the LUMO level by 50 meV and 180 meV compared to PCBM, resulting in an increase of V_{OC} by 70 mV and by 250 mV respectively in devices with the mono- and bis-adduct. These energy levels are established by cyclic voltammetry and correlated to semi-empirical quantum chemical calculations. Following the optimization of the blend morphology, critical to reach high performance, the description of optimal devices is discussed with correlation to electrical materials properties and structural characterization. Finally, we compare device performance of bis-oQDMC$_{60}$ to analogous bis-C_{60} adducts, such as bis-PCBM and indene C_{60} bis-adduct (ICBA) in similarly processed devices, in order to gain some insight as to the optimization of polymer:fullerene bulk heterojunctions.

2. Experimental

2.1. Synthesis of mono-*ortho*-quinodimethane C_{60} and bis-*ortho*-quinodimethane C_{60}

Both o-quino-dimethane derivatives were synthesized by means of a [4 + 2]-cycloaddition, modifying a procedure previously reported by Belik *et al.*[19] To a solution of C_{60} (6.0 g) in toluene (3.0 L), 1,2-bis(bromomethyl)benzene (4.44 g), potassium iodide (6.0 g), and crown-6 (36 g) were added. The reaction mixture was heated to reflux under argon in the dark for 24 h and then cooled to room temperature. The mixture was washed with NaOH (5%), water, and brine. After drying over magnesium sulfate (anhydrous), the solvent was removed under reduced pressure. Separation by flash chromatography on silica gel (230–400 mesh, 60 Å) with toluene/cyclohexane (1 : 7) as eluent, resulted in three major fractions. Analysis by means high-pressure liquid chromatography (HPLC) on an Agilent Series 1100 HPLC instrument using a 2-(1-pyrenyl)ethylsilica stationary phase (Cosmosil BuckyPrep column, 250 mm × 4.6 mm), toluene for elution (1 mL min^{-1}) and detection at 330 nm allowed for the identification of Fractions 1, 2 and 3 as unreacted C_{60} (10%), mono-*ortho*-quinodimethane C_{60} (5%) and bis-*ortho*-quinodimethane C_{60} (38%), respectively. After repeated chromatographic purification, 2.60 g of mono-oQDMC$_{60}$ and 1.40 g of bis-oQDMC$_{60}$, at purities of 99.8% and over 99.5% could be recovered. Corresponding yields relative to the initial C_{60} were 37.9 and 18.1%. HPLC chromatograms of purified mono- and bis-oQDM$_{60}$ are given in the supporting information.†

2.2. Cyclic voltammetry

Glassy carbon was used as a working electrode whereas platinum and silver wires served as counter and reference electrodes, respectively. The experiments were run in 0.05 M solutions of tetra-n-butylammonium hexafluorophosphate (TBAPF6) in *ortho*-dichlorobenzene (ODCB).

2.3. Photo-CELIV measurements

Photogenerated charge carrier extraction by linearly increasing voltage (photo-CELIV) measurements, to extract charge carrier mobility, were performed at 300 K in a closed-cycle helium cryostat on optimized photovoltaic devices with an active area of 2 mm^2 to limit resistive and capacitive artifacts. A double-pulse generator (Agilent 81150A) was used to apply a triangular voltage pulse to the solar cell. The current transients were acquired by a digital oscilloscope (Agilent Infiniium DSO90254A) after amplification by a current–voltage amplifier (FEMTO DHPCA-100). The second harmonic of a Nd:YAG laser (λ = 532 nm, < 80 ps pulse duration) was used for laser excitation. The charge carrier mobility was calculated in accordance with a previously established method.[20] As the measurements were carried out at room temperature, the extracted mobility values are considered as only lower limits of the actual values, as the photo-CELIV peak maximum was on the order of the RC time constant of the circuit.

2.4. Solubility

In a first attempt, increasing quantities of the various fullerene derivatives were dispersed by sonication then filtered. The filtrate was analyzed with HPLC using extinction coefficients determined for each compound by means of calibration curves. In all cases, the resulting solubilities appeared to depend on the initial concentrations despite indubitable saturation of the solution indicated by aggregates. One possible explanation is that sonification yielded stable suspensions instead of real solutions, hence another approach based on ASTM standard E1148 is implemented here. Solutions corresponding to concentrations higher than those observed above were prepared and stirred for more than 3 days at room temperature in order to achieve equilibrium. For this purpose, 1.003 g of PCBM, 4.008 g of bis-PCBM, 0.32198 g of mono-oQDMC60, 2.558 g of bis-oQDMC60 and 3.507 g of ICBA were added to 10 mL of ODCB, respectively. Samples of 1 to 2 mL were taken after 90, 94 and 96 h, filtered through a 0.2 mm pore size syringe filter, diluted 50 : 1 with ODCB and analyzed by means of HPLC. Solids remained in each flask indicating that saturation was achieved. Concentrations determined at the three sampling times varied slightly but not systematically, indicating that equilibrium was reached.

2.5. Thin film characterization

Absorption spectra of the films on quartz substrates were measured between 250 and 900 nm with a Shimadzu UV-1601PC UV-visible spectrophotometer. Out-of-plane ordering of the spin-coated thin films was examined by X-ray reflectivity (XRR) involving $\theta/2\theta$ scans on a PANalytical XPert Pro Materials Research Diffractometer using CuKα radiation. An integration time of 5 s per 0.01° was used. Measurements were performed on films prepared under the same conditions as solar cells, except on SiO_2 substrates. Atomic force microscopy (AFM) topography and phase scans were recorded directly on devices using a Picoscan PicoSPM LE scanning probe in tapping mode.

2.6. Device processing and characterization

Solar cells were prepared on glass substrates coated with patterned indium-tin-oxide (ITO) with a sheet resistance of 15 Ω sq^{-1}. Substrates were thoroughly cleaned in a sequence of sonication in detergent, deionized water, acetone and isopropanol, and finally treated with ultraviolet-ozone for 15 min. First, filtered PEDOT:PSS (Baytron P VPAl4083) was spin-coated at 5000 rpm for 60 s, giving a 25 nm thick layer. Then, samples were transferred to a nitrogen filled glovebox where they were annealed at 130 °C for 10 min to remove excess water. All further steps of processing, sample transfer and characterization were carried out in an inert nitrogen atmosphere. P3HT (Sepiolid P200, Rieke Metals) and all C_{60} derivatives (PCBM, bis-PCBM, mono-oQDMC$_{60}$ and bis-oQDMC$_{60}$) were synthesized at Nano-C, Inc. with purities of 99.5%. Mono-PCBM is a standard commercial product (www.nano-c.com) and bis-PCBM is a by-product recovered during its chromatographic purification. ICBA was purchased from Lumtec. A solution of 2.5 wt% in ODCB in a 1 : 0.8 or 1 : 1.2 ratio was used for mono-adducts and bis-adducts, respectively. Mono-o-quino-dimethane C_{60} was dissolved in a mixture of ODCB and chlorobenzene. The solutions were stirred inside the glovebox at 80 °C overnight. In some cases 1,8-octanedithiol is added to the dissolved ink in 0.5 μL mg^{-1} of fullerene weight. The active layer was spin-coated at 600 rpm for 40 s, and the still wet film was covered with a petri dish for 30–40 min. The samples were subsequently heated at 130 °C and 170 °C for 10 min in the case of PCBM and the bis-adducts, respectively, to achieve an optimal morphology. The cathode composed of 20 nm of Ca and 100 nm of Al was deposited at 10^{-7} mbar with a 1.5 Å s^{-1} deposition rate. The metals evaporated through a shadow mask defined eight cells of 32 mm^2 on each substrate. The actual active area was measured using an optical microscope. The initial photovoltaic characteristics were measured in inert atmosphere with a Keithley 2602A in two-wire configuration under an Abet Xenon arc lamp with 100 mW cm^{-2} illumination intensity and AM1.5G spectrum. The lamps' intensity was calibrated with an ISE Fraunhofer certified Si photodiode. For external quantum efficiency measurement, light from Xe and quartz halogen lamps was coupled into a monochromator and their intensities were calibrated with a Si photodiode. The light incident on the device was chopped and the modulated current signal was detected with a current–voltage and lock-in amplifier.

3. Results and discussion

In this section, we first present various properties of mono- and bis-oQDMC$_{60}$ relevant to photovoltaic performance, such as energy levels, charge carrier mobility and solubility in a common chlorinated organic solvent. This is followed by the optimization of the P3HT:bis-oQDMC$_{60}$ morphology, crucial to achieve high performance. Next, optimized photovoltaic devices utilizing mono- and bis-oQDMC$_{60}$ derivatives in photovoltaic devices are reported. Finally, we draw comparisons between bis-oQDMC$_{60}$ and two other bis-adducts, namely bis-PCBM and ICBA. Chemical structures of all molecules discussed in this article are depicted in Fig. 1.

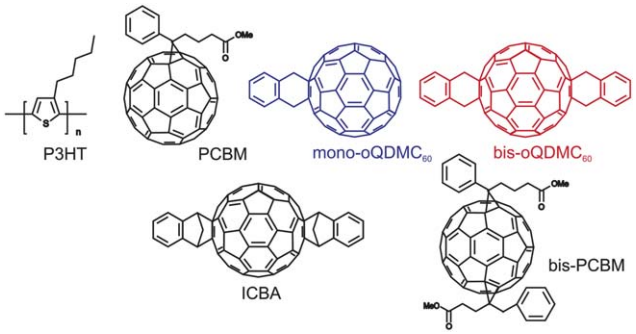

Fig. 1 Chemical structures of P3HT and the various fullerene derivatives discussed in this article, namely PCBM, mono- and bis-o-quinodimethane C_{60}, bis-PCBM and ICBA.

3.1. Materials properties of the fullerenes

The electronic structure of the fullerene derivatives has been assessed both computationally and *via* electrochemical techniques. As hardware requirements as well as computation time increase exponentially with the number of electrons, semi-empirical quantum chemical techniques have been used in the present work. All results reported here have been obtained by means of the PM3 method using the Hyperchem 8.0 software package.[21] Taking into account that discrepancies with

Table 1 Lowest unoccupied molecular orbital (LUMO) of the fullerene derivatives calculated by semi-empirical quantum chemical techniques and measured by cyclic voltammetry. The LUMO of P3HT is also given for comparison[22]

Material	LUMO (eV) calculated	LUMO (eV) measured
PCBM	−4.30	−4.30
Mono-oQDMC$_{60}$	−4.27	−4.25
Bis-oQDMC$_{60}$	(−4.02)–(−4.16)	−4.12
Bis-PCBM	(−4.10)–(−4.27)	−4.18
ICBA	(−4.02)–(−4.14)	−4.06
P3HT	—	−3.4

Table 2 Mobility values measured in P3HT:fullerene blends by CELIV at room temperature

C_{60} derivative	CELIV mobility (cm^2 V^{-1} s^{-1})
PCBM	1.0×10^{-3}
Mono-oQDMC$_{60}$	2.0×10^{-3}
Bis-oQDMC$_{60}$	7.1×10^{-4}
Bis-PCBM	6.0×10^{-4}

Table 3 Solubility limit of fullerene derivatives in ODCB at room temperature determined following ASTM E1148

C_{60} derivative	*ortho*-dichlorobenzene (mg mL^{-1})
PCBM	14.1 ± 0.4
Mono-oQDMC$_{60}$	2.8 ± 0.04
Bis-oQDMC$_{60}$	61.1 ± 8.9
Bis-PCBM	147.0 ± 6.9
ICBA	140.5 ± 6.2

Table 4 Photovoltaic properties of ITO/PEDOT:PSS/P3HT:bis-oDMC$_{60}$/Ca/Al devices prepared in different drying conditions with and without 1,8-octanedithiol (OT). Values are averages and standard deviations over 6–8 devices

	Processing	V_{OC} (mV)	J_{SC} (mA cm^{-2})	FF (%)	η (%)
Bis-oQDMC$_{60}$ without OT	Fast drying	799 ± 18	5.7 ± 0.6	52 ± 3	2.3 ± 0.3
	Slow drying	834 ± 4	7.6 ± 0.4	68 ± 1	4.4 ± 0.2
Bis-oQDMC$_{60}$ with OT	Fast drying	806 ± 3	9.0 ± 0.3	62 ± 1	4.5 ± 0.2
	Slow drying	812 ± 8	8.2 ± 0.5	69 ± 2	4.6 ± 0.2

experimental data are likely to be caused by the degree of curvature of fullerenes and its effect on molecular orbital overlap and that all molecules assessed here have the same C_{60} core structure, all computed LUMO levels have been adjusted by −1.491 eV. This approach allows us to align the LUMO level of PCBM with its previously reported value of −4.30 eV.[22] Resulting LUMO levels for all molecules investigated here are given in Table 1. Due to the presence of several isomers and the challenge to identify specific isomers and their relative abundance formed in the synthesis, all theoretically possible isomers have been investigated and the lowest as well as highest LUMO level given. Lower (*i.e.*, less negative) LUMO levels for bis- compared to mono-functionalized C_{60}, as found for all species investigated here, are in agreement with previous reports.[10,17]

For experimental validation, first half-wave reduction potentials, reflecting the energy level of the LUMO, have been measured for all derivatives studied here using cyclic-voltammetry (CV). All samples were referenced to ferrocene, which was set at 0 V, as an internal standard. Similar to the approach described above for the semi-empirical computations, the LUMO level of PCBM was set to −4.30 eV while the corresponding values for the other compounds were determined based on the differences of the reduction potentials. While the resolution of CV appears not to be sufficient to differentiate between isomers, the results given in Table 1 fall within the bandwidth of the computationally obtained values and confirm at least the internal consistency of our work. Experimental uncertainties of the CV measurements were found to be less than 0.1 eV. The cyclic voltammograms are reported in the supplementary information.†

The electron mobility of the acceptor is another important parameter, as poor charge carrier transport can limit device performance. In organic solar cells, the mobility in the vertical direction through a network of fullerenes included in the polymer matrix is a particularly pertinent value. Photo-CELIV allows one to measure this mobility directly in solar cells, though it should be noted the values represented in Table 2 express a combined mobility of holes and electrons, as both contribute to the extraction peak in the photo-CELIV experiment.[20] As the donor material, P3HT, is identical in all blends, values reflect the differences in fullerene mobility. The mobility in mono-oQDMC$_{60}$ is even slightly higher than that of PCBM, whereas bis-oQDMC$_{60}$ has a 40% lower mobility. Similarly, bis-PCBM also possesses a reduced mobility compared to its mono-adduct. Bis-adducts are inherently composed of various isomers, resulting in an energetic disorder that may hinder charge transport.

Finally, it is important to evaluate the solubility of various fullerenes, as this could impact ink formulation and film forming. Solubility directly determines the dynamics of aggregation during film forming. As P3HT:fullerene blends are often casted from ODCB, room temperature solubility is determined following a standardized procedure in this solvent and listed in Table 3. Even though mono-oQDMC$_{60}$ has the lowest solubility in ODCB, which is considered to limit device performance, we present in the next section that a solvent mixture is still able to ensure over 4% device efficiency.[23] Bis-oQDMC$_{60}$ has a 4-fold higher solubility than PCBM, similar to other bis-adducts.

Optical absorption of the mono- and bis-oQDMC$_{60}$ are similar to that of PCBM and bis-PCBM, we do not observe an increased absorption in the visible region by the o-quino-dimethane sidechains compared to PCBM's sidechain as presented in the supplementary information.†

3.2. Photovoltaic device optimization

In order to present a meaningful comparison to PCBM, first the formulation of the ink and the deposition of the photoactive blend need to be adapted for these new C_{60} derivatives.

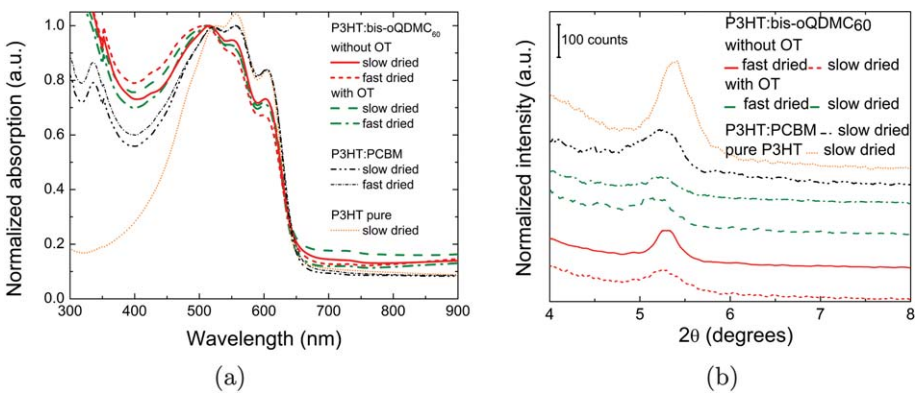

Fig. 2 (a) Normalized UV-visible spectra of P3HT:bis-oQDMC$_{60}$ layers slow and fast dried with and without 1,8-octanedithiol (OT) prior to thermal annealing. As a reference, the absorption of pure P3HT and P3HT:PCBM are also depicted. (b) XRR patterns of the corresponding layers.

Bis-oQDMC$_{60}$, especially, requires significant consideration to preserve a high J_{SC} and FF, involving the adjustment of the polymer:fullerene ratio, spin-coating conditions, and solvent and thermal annealing applied prior to metallization. Finally, the influence of processing additives is also briefly explored. We examine the effect of these various parameters both on the electrical properties of the devices and on the blend morphology by absorption spectroscopy and X-ray reflectivity (XRR) in order to probe the bulk, whereas film topography is monitored by AFM. For comparison, all layers were processed under identical conditions with a thickness of 170–180 nm. As a reference, P3HT:PCBM layers and devices are prepared under identical processing conditions.

Firstly, P3HT:fullerene weight ratio is adjusted by slightly varying the ratio between 1 : 0.8 and 1 : 1.4. The optimal 1 : 1.2 ratio is established by a trade-off between the steadily rising FF values from 60% to 69% and the drop in V_{OC} from 835 mV to 815 mV with increasing fullerene loading (Fig. S5(a) in the supporting information†). As the molecular weight of bis-oQDMC$_{60}$ is only 1% higher compared to PCBM, maintaining the optimal molarity ratio between P3HT and fullerene cannot account for this improvement. Furthermore, absorption spectroscopy indicates that this optimal ratio slightly impedes P3HT crystallization, illustrated by a decrease of the characteristic shoulder at a wavelength of 620 nm (Fig. S5(b) in the supporting information†).[24] Hence we tentatively attribute the enhanced FF with increasing fullerene loading to improved electron transport.

Secondly, solvent annealing, also referred to as slow drying, has proven to be a crucial step to achieve enhanced performance. The impact of this process has been extensively investigated in P3HT:PCBM devices, and has resulted in the highest reported efficiencies.[25,26] However, solvent annealing of P3HT:bis-oQDMC$_{60}$ blends results in a two-fold enhancement, whereas reference P3HT:PCBM samples only exhibit a 10% increase in efficiency as reported in Table 4. The high regioregularity of the P3HT (>98%) used here explains the reduced influence of solvent annealing in the P3HT:PCBM blend reference. In contrast to blends with PCBM, absorption spectroscopy reveals a significantly reduced P3HT crystallization in fast dried films with bis-oQDMC$_{60}$, indicated by the diminished vibronic features of P3HT at wavelengths of 550 nm and 620 nm, as shown in Fig. 2 (a). One could also observe that, even in solvent annealed films, bis-oQDMC$_{60}$ seems to considerably impede P3HT organization when compared to a blend with PCBM. At first sight however, XRR measurements of corresponding films, depicted in Fig. 2 (b), indicate larger crystallites in fast dried layers, namely 32 nm compared to 23 nm in slow dried films as estimated by the Scherrer equation.[27] Crystallographic data extracted from the peak fitting of the XRR results are listed in the supporting information.† However, XRR probes the out-of-plane ordering of polycrystalline P3HT, but does not account for crystallites with stacking order other than vertical, which tend to develop in solvent annealed layers.[28] Besides, AFM topography and phase images shown in Fig. 3, which are strongly linked to the bulk morphology, indicate that the fast dried films, indeed, exhibit large, straight chain-like domains, whereas the slow dried films have homogeneously mixed small domains.[25] In these images, the fibrillar features are assigned to P3HT crystallites, while the domains in between appear to be amorphous. Additionally, the slow dried layers have a rougher interface on a longer scale compared to the fast dried films with a short scale reduced roughness, in agreement with previous reports.[25]

Hence, AFM phase images in correlation with XRR measurements reveal larger P3HT crystallites when layers are dried fast, while slow drying permits the formation of P3HT crystallites in finely intermixed phases. Previous grazing-incidence X-ray diffraction studies confirmed that even though fast drying results in larger domains, the overall crystallinity is generally enhanced with slow drying, as we can also observe with absorption spectroscopy.[28] These observations aligned with earlier studies on P3HT:PCBM blends allow us to understand the difference in phase segregation between blends with bis-oQDMC$_{60}$ and PCBM. Li *et al.*, described that slow drying permits the diffusion and aggregation of the fullerene molecules intermixed with P3HT chains, thus allowing P3HT to locally self-organize and crystallize. Therefore, we consider that the strong influence of the drying conditions on the blend morphology arises from the fact that bis-oQDMC$_{60}$ remains finely dispersed in the film and thus inhibits the nanoscale aggregation necessary for phase segregation. We attribute this enhanced intermixing of the fullerene in the film to its considerably enhanced solubility in ODCB. While PCBM is often deposited from a solution at close to its solubility limit, conditions for aggregation are rapidly reached, whereas the same situation may not occur during film formation with bis-oQDMC$_{60}$. Besides, the higher optimal fullerene loading in blends also indicates that the aggregation and the formation of the percolating fullerene network are hindered. This relationship between the fullerenes solubility and

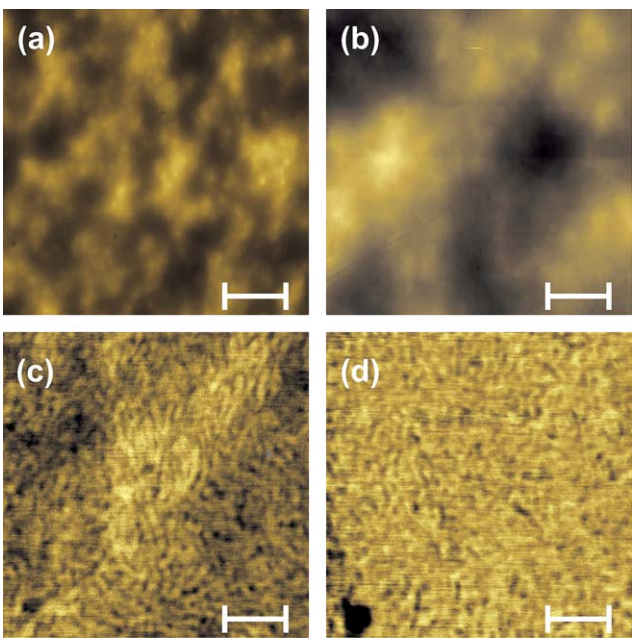

Fig. 3 AFM topography images of 2.5 μm × 2.5 μm areas of films deposited on ITO glass covered with PEDOT:PSS, and the P3HT:bis-oQDMC$_{60}$ blends that are either fast (a) or slow dried (b). The rms roughness of the films are 11 nm and 17 nm, respectively. The horizontal scale bars are 500 nm. Corresponding AFM phase images of 500 nm × 500 nm areas of the same films are shown for fast (c) and slow dried (d) films. The horizontal scale is 100 nm in this case.

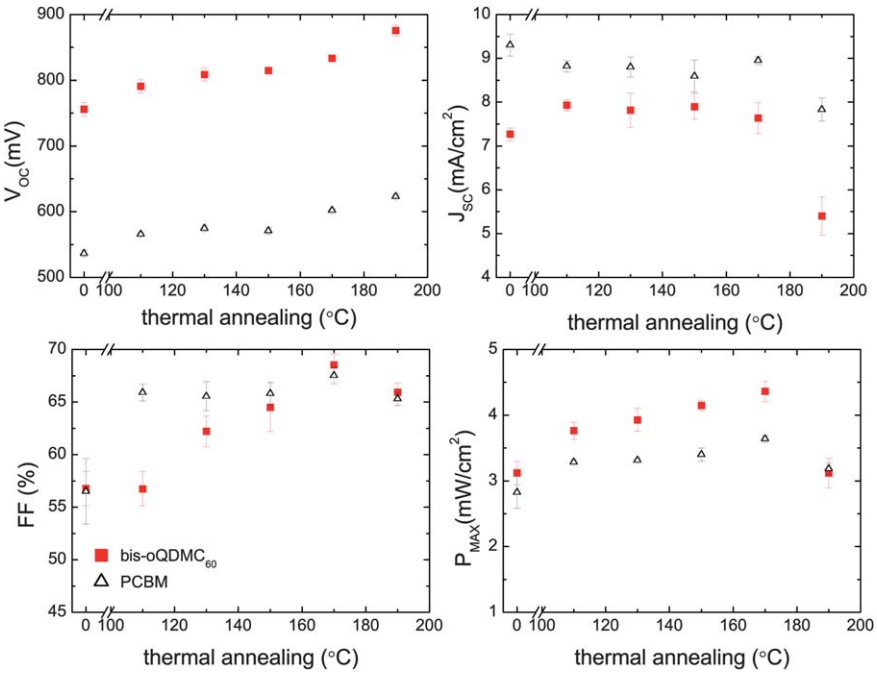

Fig. 4 Evolution of the photovoltaic parameters as a function of the temperature of thermal annealing in P3HT:PCBM and P3HT:bis-oQDMC$_{60}$ devices. The thermal annealing was applied after the solvent annealing for 10 min.

blend morphology not only assists further optimization in this case but can also serve as a guide for similar bis-fullerene adducts, which inherently present an increased solubility compared to their mono-adducts.

Similarly enhanced fullerene aggregation can also be achieved with processing additives incorporated in P3HT:PCBM blends, thus they present an alternative to solvent annealing as previously shown by Yao *et al.*[26] We found the incorporation of octanedithiol (OT) allowed a successful substitution of the solvent annealing as the photovoltaic parameters in Table 4 show. We achieved higher J_{SC} and similar FF compared to solvent annealed devices, though reduction of V_{OC} counterbalances this improvement, resulting in a similar performance under both processing conditions. The optical and structural characterization presented in Fig. 2 also confirm that both processing routes lead to similar P3HT ordering and crystallization. The enhanced photovoltaic properties achieved by additives promoting fullerene aggregation further proves that optimal phase segregation is limited by the fine dispersion of the fullerene in the blend.

The last step of the morphology optimization involved the determination of the optimal annealing temperature. Unlike in P3HT:PCBM films, blends with bis-oQDMC$_{60}$ present a clear optimum at an annealing temperature of 170 °C as presented in Fig. 4. This results from the steadily increasing FF with annealing temperature, whereas the FFs in P3HT:PCBM blends plateau above 110 °C. Thermal annealing in P3HT:fullerene blends equally contributes to the crystallization of the polymer and the formation of PCBM aggregates.[29] Absorption spectroscopy, presented in Fig. S7 in the supporting information,† indicates that P3HT crystallization progresses little over 110 °C in both cases, and this is also supported by the stable J_{SC} over

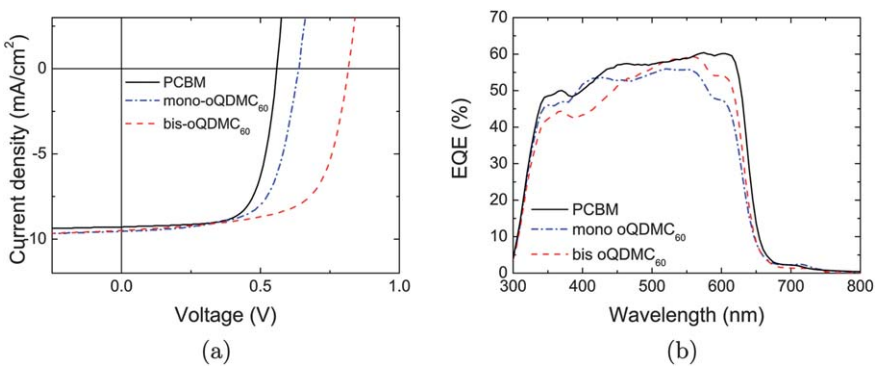

Fig. 5 (a) Current density *vs.* voltage characteristics under 100 mW cm^{-2} AM1.5G simulated solar illumination and (b) external quantum efficiency (EQE) measurement of solar cells where P3HT is blended with the different fullerene derivatives. The device structure consists of ITO/PEDOT:PSS/blend/Ca/Al.

Table 5 Photovoltaic properties of devices reported in Fig. 5 and 6. Values given are best, while averages over 6–8 devices are given in parentheses

C_{60} derivative	V_{OC} (mV)	J_{SC} (mA cm^{-2})	FF (%)	η (%)
PCBM	567 (561)	9.6 (9.5)	70 (68)	3.8 (3.6)
Mono-oQDMC$_{60}$	639 (638)	9.5 (9.4)	67 (64)	4.1 (3.9)
Bis-oQDMC$_{60}$	816 (818)	9.4 (9.0)	66 (65)	5.2 (5.1)
Bis-PCBM	686 (685)	9.4 (9.1)	65 (65)	4.2 (4.1)
ICBA	828 (819)	9.7 (9.5)	69 (70)	5.6 (5.4)

different annealing temperatures. Thus, the higher optimal annealing temperature suggests both an initially more dispersed fullerene network and higher glass transition temperature of the blend film.

Unlike bis-oQDMC$_{60}$, its mono-adduct required only slight adaptation of the ink formulation, due to its reduced solubility in ODCB. A mixture of chlorobenzene and ODCB deposited from hot solution allowed us to prepare 180–220 nm thick particle-free films with a close to optimal morphology.

Finally the optimized photovoltaic performance of bulk heterojunction solar cells made with the various C_{60} derivatives and regioregular P3HT is compared in Fig. 5 and in Table 5. Devices with similar layer thicknesses of 220–240 nm are compared, although processing conditions differ slightly for the various fullerenes. Their performance reaches 4.1% and 5.2% with the mono- and the bis-oQDMC$_{60}$, respectively, compared to 3.8% obtained with PCBM. This improvement is solely due to an increase of 75 mV and 250 mV in V_{OC} as both the J_{SC} and FF remain nearly unchanged. Furthermore, the shift of the LUMO levels by 50 meV and 180 meV correlates well with the increase of V_{OC}. Our optimal P3HT:PCBM devices achieve a FF of over 70% even in thicker layers, while blends with bis-oQDMC$_{60}$ only have similarly high FF in thinner films of 150–180 nm. We attribute this limitation in FF mostly to hindered phase segregation and not to reduced electron mobility.

Moreover, the spectral response shown in Fig. 5 (b) also reveals variations in the morphology in the blends with the new fullerenes, as the characteristic vibronic features of P3HT differ in comparison to the blend with PCBM,[30] in agreement with the previously presented absorption spectroscopy results.

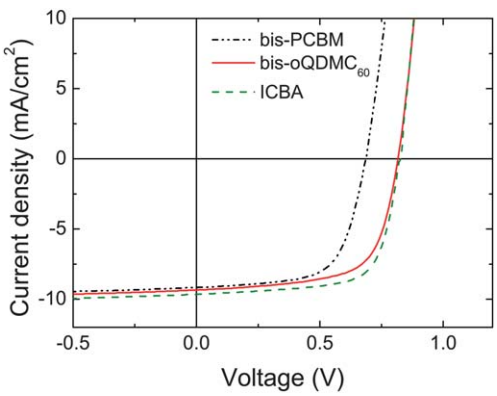

Fig. 6 Current density *vs.* voltage characteristics under 100 mW cm^{-2} AM1.5G simulated solar illumination of devices blended with P3HT and bis-PCBM, bis-oQDMC$_{60}$ and ICBA.

3.3. Comparison to other bis-adducts

This investigation of bis-oQDMC$_{60}$ is further completed by comparison of its photovoltaic parameters with those of analogous bis-adducts. For this, devices with identical device architecture and ink formulation, as well as similar blend thickness of 200 nm are prepared. Additionally, all bis-adducts present an increased solubility compared to the mono-adduct as listed in Table 3, resulting in the similar difficulty to achieve an optimal morphology. Therefore, applying the same processing conditions for all bis-adducts yields close to optimal devices and it further increases the relevance of the comparison.

As Fig. 6 and Table 5 show, J_{SC} in all devices remain similar, whereas V_{OC} increases to 690 mV, 820 mV, 830 mV for bis-PCBM, bis-ODMC$_{60}$ and ICBA, respectively, compared to 570 mV for PCBM. These values are in agreement with the shift of the molecule's LUMO by 120 meV, 220 meV and 240 meV as determined by cyclic voltammetry and confirmed by computation, as shown in Table 1. Interestingly, the minor distinctions between bis-oQDMC$_{60}$ and ICBA induces not only a shift in V_{OC} but also enhanced FF with ICBA, yielding the highest efficiency of 5.6%. The higher FF achieved with ICBA suggests improved charge transport, though it cannot be discerned whether it originates from the impact of blend morphology and/or intrinsic properties of the fullerenes. One drawback of these sidechains attached to the C_{60} cage is their reduced absorption in the visible spectrum compared to C_{60} as shown in the supplementary information.† The minor differences in J_{SC} are only due to slight differences in P3HT organization in the various blends. High photocurrent in these devices with V_{OC} > 800 mV also indicates that further efficiency improvements remain possible by energy level engineering of the P3HT: fullerene material system.

4. Conclusions

Here, we have described the implementation in photovoltaic devices of a novel fullerene derivative, o-quino-dimethane C_{60}, in its mono and bis-adduct form. The latter yields up to 5.2% efficient devices in blends with P3HT, due to its considerably higher LUMO levels achieved by bis-adduction of the compact o-quino-dimethane sidechain. In agreement with previous reports, this design route preserves high charge carrier mobility and careful optimization of the phase segregation also maintains a high photocurrent. Hindered phase segregation of the photo-active blend due to the increased solubility of the bis-adduct is corrected by thermal and solvent annealing or alternatively by the use of solvent additives. The morphology optimization presented here can serve as a guide for the preparation of similar blends of P3HT and bis-fullerene adducts, which inherently possess a higher solubility. Comparison of bis-o-quino-dimethane C_{60} to analogous bis-adducts show its superior performance compared to bis-PCBM due to its increased energy level, while its performance is comparable to ICBA. As with ICBA, high V_{OC} is achieved without any reduction in J_{SC}, indicating that a reduction of the offset between LUMO levels from 900 meV to 600 meV still allows an efficient photocurrent generation. Hence, both bis-oQDMC$_{60}$ and ICBA yield a considerably enhanced device efficiency compared to PCBM, and also suggest that

further improvement by energy level engineering of fullerene derivatives is still possible.

Acknowledgements

The authors thank C. Girotto for AFM measurements. K. V. acknowledges the Institute for the Promotion of Innovation through Science and Technology in Flanders (IWT-Vlaanderen) for financial support. The work of A. B. and C. D. is supported by the Bundesministerium für Bildung und Forschung in the framework of the GREKOS project (contract no. 03SF0356B). A. B. thanks the German Federal Environmental Foundation (Deutsche Bundesstiftung Umwelt) for funding. C. D. gratefully acknowledges the support of the Bavarian Academy of Sciences and Humanities.

References

1 NREL certificate of 8.3% efficiency, Konarka press release, 2010.
2 R. F. Service, *Science*, 2011, **332**, 293.
3 Y. J. Cheng, S. H. Yang and C. S. Hsu, *Chem. Rev.*, 2009, **109**, 5868–5923.
4 J. E. Anthony, A. Facchetti, M. Heeney, S. R. Marder and X. Zhan, *Adv. Mater.*, 2010, **22**, 3876–3892.
5 T. M. Clarke and J. R. Durrant, *Chem. Rev.*, 2010, **110**, 6736–67.
6 C. J. Brabec, A. Cravino, D. Meissner, N. S. Sariciftci, M. T. Rispens, L. Sanchez, J. C. Hummelen and T. Fromherz, *Thin Solid Films*, 2002, **403–404**, 368–372.
7 J. E. Anthony, *Chem. Mater.*, 2011, **23**, 583–590.
8 A. Varotto, N. D. Treat, J. Jo, C. G. Shuttle, N. A. Batara, F. G. Brunetti, J. H. Seo, M. L. Chabinyc, C. J. Hawker, A. J. Heeger and F. Wudl, *Angew. Chem., Int. Ed.*, 2011, **50**, 5166–5169.
9 S. A. Backer, K. Sivula, D. F. Kavulak and J. M. J. Frechet, *Chem. Mater.*, 2007, **19**, 2927–2929.
10 M. Lenes, G. J. A. H. Wetzelaer, F. B. Kooistra, S. C. Veenstra, J. C. Hummelen and P. W. M. Blom, *Adv. Mater.*, 2008, **20**, 2116–2119.
11 J. A. Mikroyannidis, A. N. Kabanakis, S. S. Sharma and G. D. Sharma, *Adv. Funct. Mater.*, 2011, **21**, 746–755.
12 D. W. Laird, R. Stegamat, H. Richter, V. Vejins and L. Scott, T. A. Lada, Patent application wo 2008/018931 a2., 2008.
13 Y. He, H.-Y. Chen, J. Hou, Y. Li and J. Am, *J. Am. Chem. Soc.*, 2010, **132**, 1377–1382.
14 G. Zhao, Y. He and Y. Li, *Adv. Mater.*, 2010, **22**, 4355–4358.
15 R. B. Ross, C. M. Cardona, F. B. Swain, D. M. Guldi, S. G. Sankaranarayanan, E. Van Keuren, B. C. Holloway and M. Drees, *Adv. Funct. Mater.*, 2009, **19**, 2332–2337.
16 M. Liedtke, A. Sperlich, H. Kraus, A. Baumann, C. Deibel, M. Wirix, J. J. Loos, C. Cardona and V. Dyakonov, *J. Am. Chem. Soc.*, 2011, **133**, 9088–9094.
17 J. M. Frost, M. A. Faist and J. Nelson, *Adv. Mater.*, 2010, **22**, 4881–4884.
18 J. Schafferhans, C. Deibel and V. Dyakonov, *Adv. Energy Mater.*, 2011, **1**, 655–660.
19 P. Belik, A. Gigel, J. Spickerniunn and K. Millen, *Angew. Chem., Int. Ed. Engl.*, 1993, **32**, 78–80.
20 J. Lorrmann, B. H. Badada, O. Inganäs, V. Dyakonov and C. Deibel, *J. Appl. Phys.*, 2010, **108**, 113705.
21 Hyperchem 8.0, Hypercube, Inc., 2007.
22 M. Scharber, D. Muhlbacher, M. Koppe, P. Denk, C. Waldauf, A. J. Heeger and C. J. Brabec, *Adv. Mater.*, 2006, **18**, 789–794.
23 P. A. Troshin, H. Hoppe, J. Renz, M. Egginger, J. Y. Mayorova, A. E. Goryachev, A. S. Peregudov, R. N. Lyubovskaya, G. Gobsch, N. S. Sariciftci and V. F. Razumov, *Adv. Funct. Mater.*, 2009, **19**, 779–788.
24 P. J. Brown, S. D. Thomas, A. Kohler, J. S. Wilson, J. Kim, C. M. Ramsdale, H. Sirringhaus and R. H. Friend, *Phys. Rev. B: Condens. Matter*, 2003, **67**, 064203.
25 G. Li, V. Shrotriya, Y. Yao, J. Huang and Y. Yang, *J. Mater. Chem.*, 2007, **17**, 3126–3140.
26 Y. Yao, J. Hou, Z. Xu, G. Li and Y. Yang, *Adv. Funct. Mater.*, 2008, **18**, 1783–1789.
27 T. Erb, U. Zhokhavets, G. Gobsch, S. Raleva, B. Stuhn, P. Schilinsky, C. Waldauf and C. Brabec, *Adv. Funct. Mater.*, 2005, **15**, 1193–1196.
28 G. Li, Y. Yao, H. Yang, V. Shrotriya, G. Yang and Y. Yang, *Adv. Funct. Mater.*, 2007, **17**, 1636–1644.
29 T. Agostinelli, S. Lilliu, J. G. Labram, M. Campoy-Quiles, M. Hampton, E. Pires, J. Rawle, O. Bikondoa, D. D. C. Bradley, T. D. Anthopoulos, J. Nelson and J. E. Macdonald, *Adv. Funct. Mater.*, 2011, **21**, 1701–1708.
30 P. Vanlaeke, A. Swinnen, I. Haeldermans, G. Vanhoyland, T. Aernouts, D. Cheyns, C. Deibel, J. D'Haen, P. Heremans, J. Poortmans and J. Manca, *Sol. Energy Mater. Sol. Cells*, 2006, **90**, 2150–2158.

